Journal of Molecular Liquids 248 (2017) 302–313

Contents lists available at ScienceDirect

Journal of Molecular Liquids

journal homepage: www.elsevier.com/locate/molliq

A facile synthesis of mordenite zeolite nanostructures for efficient bleaching of crude soybean oil and removal of methylene blue dye from aqueous media

Mostafa Y. Nassar [a,*], Ehab A. Abdelrahman [a], Ahmed A. Aly [b], Talaat Y. Mohamed [a]

[a] Chemistry Department, Faculty of Science, Benha University, Benha 13518, Egypt
[b] Home Economics Department, Faculty of Specific Education, Benha University, Benha 13518, Egypt

ARTICLE INFO

Article history:
Received 6 May 2017
Received in revised form 7 October 2017
Accepted 12 October 2017
Available online 14 October 2017

Keywords:
Nano-sized mordenite
Hydrothermal synthesis
Soybean oil
Bleaching
Methylene blue
Water treatment

ABSTRACT

In the current investigation, we have reported on the preparation of mordenite zeolite nanostructures using a low-cost hydrothermal treatment of silica gel, aluminum nitrate, and sodium hydroxide. The influence of organic templates such as ethylene glycol, glycerol, and polyethylene glycol 200 (PEG 200) on the zeolite products was studied. The crystallite sizes of the as-fabricated samples increased in the following order: (PEG 200) < (ethylene glycol) < (glycerol) < (without template). The PEG 200 organic template generated a mordenite product with 57.51 nm crystallite size and 28.26 m^2/g BET surface area. The as-prepared products were identified using FE-SEM, FT-IR, XRD, HR-TEM, and BET analysis. The as-prepared mordenite product could be successfully applied to purify the crude soybean oil from the yellow and red colors. The mordenite product also showed good adsorption properties toward the removal of methylene blue (MB) dye from wastewater. Kinetic data exhibited that the dye adsorption process obeyed pseudo-first-order, intra-particle diffusion, liquid film diffusion, and pore diffusion models whereas the rate determining step of the adsorption is only controlled by the pore diffusion model. Adsorption data fitted well both Langmuir and Dubinin–Radushkevich (D–R) isotherm models. Moreover, the adsorption is a physisorption and exothermic process.

1. Introduction

In the past few years, a considerable attention has been paid to oils and fats because they are the most main gradients of human foods that are necessary for the continuation of human life. This is owing to their importance as antioxidant and vitamin generator components [1]. Oils and fats can be categorized into two main categories based on their main sources; animal and plant sources. The plant sources are produced from the plant seeds such as cotton, soybean, sesame, grapes, etc. [2]. Those crude plant oils contain undesired and dangerous colored compounds to human health; particularly, the red and yellow colored species [3]. One of the most important stages of refining processing of the crude oils is bleaching designed to remove colored compounds using bleaching earth materials composed of silicon and aluminum oxides due to their high adsorption capacities [4]. In this light, some bleaching earth powders have been used for bleaching several oils such as cottonseed oil, soybean oil, hazelnut oil, rapeseed oil, sardine oil, and palm oil [5–10].

The bleaching earth powders, applied to bleach the vegetable oils, are composed of clays activated by acid treatment. In this vein, attapulgite, bentonite, and sepiolite have been reported for the removal of pigments from oils through the adsorption process [6,11]. However, most of the aforementioned bleaching earth powders have some drawbacks such as high-cost production, need some chemical treatments and these are highly cost (expensive), low or moderate adsorption efficiency and/or generating several pollutants during their production. Therefore, the development of new adsorbents with high surface area, having an excellent bleaching efficiency, is still a challenge. Recently, researchers have devoted their effort to producing nanomaterials and applying them as nano-adsorbents due to their high surface areas. Among those nanomaterials, zeolites have attracted the attention of many scientists due to their high surface area, and low- cost production, and stability in water. Mordenite is one of the most important type of zeolites composed of silicon and aluminum oxides and it has a composition $Na_8Al_8Si_{40}O_{96}\cdot nH_2O$.

On the other hand, water pollution with various dyes (including methylene blue (MB)) discharged by different industries is a serious problem due to the non-biodegradability, chemically stability, and toxicity of most of the discharged dyes [12]. These pollutants have negative effects on the human health such as respiratory irritation, issues chemical burns, etc. [13,14]. Consequently, the removal of these pollutants from wastewaters is a crucial necessity for our environment. So far, various routes have been suggested for the removal of organic

* Corresponding author.
E-mail addresses: m_y_nassar@fsc.bu.edu.eg, m_y_nassar@yahoo.com (M.Y. Nassar).

https://doi.org/10.1016/j.molliq.2017.10.061
0167-7322/

contaminants from wastewaters. And these methods include ozonation, membrane separation, biological treatment, ultra-sonication, coagulation, photocatalysis, and adsorption [12,15–30]. However, adsorption has the superiority over the other methods due to its high efficiency, simplicity, scalability, and economic applicability [31,32]. The focus of the recent research has been on zeolites, especially mordenite, as nano-adsorbents owing to the aforementioned characteristics and their various applications such as catalysis [33] and cumene production [34], as well as adsorption of inorganic and organic pollutants [35–37]. Recently, mordenite and its nanocomposites have proven its efficiency as nano-adosbents for the removal of various environmentally organic and inorganic contaminants and the corresponding isotherm models have been reported [38–42]. Moreover, reports on the synthesis of mordenite nanoparticles via inexpensive routes are limited [42–50]. However, the methods reported in the literatures have many disadvantages such as using highly cost silicon sources (tetraethylorthosilicate, fumed silica, sodium silicate, colloidal silica, and silicic acid) and/or expensive templates (*o*-phenylenediamine and tetraethylammonium hydroxide). The hydrothermal method has proven its efficiency in producing various nanomaterials [15,29,30,51,52]. Therefore, developing a new, facile and low-cost procedure for preparation of mordenite nanoparticles and applying the prepared nanostructures to bleach soybean oil and to remove MB dye from aqueous media were necessary. Hence, in the present investigation, we develop a new and facile method for the preparation of mordenite zeolite using silica gel as an inexpensive silicon source and inexpensive template sources such as ethylene glycol, glycerol and polyethylene glycol 200. The as-prepared mordenite zeolite was used as a nanoadsorbent for bleaching the crude soybean oil. The as-prepared mordenite nanostructure was also used for the removal of MB dye from polluted waters.

2. Experimental

2.1. Chemicals

The chemicals such as sodium hydroxide (NaOH), silica gel (SiO_2), and aluminum nitrate ($Al(NO_3)_3(H_2O)_9$) that were used in this research have a high purity and were purchased from Sigma-Aldrich Company. The crude soybean oil and bleaching earth were kindly supplied by Tanta Company for oils and soaps, Egypt.

2.2. Synthesis of mordenite zeolite nanoparticles

9.22 g of silica gel and 12.00 g of sodium hydroxide were dissolved in 350 mL bidistilled water upon heating, and this solution was labeled as solution A. An aqueous solution of aluminum nitrate, 75.0 mL, (0.53 g, 1.4 mmol) was added drop wise to 75 mL of solution A, and the reaction blend was stirred for 1 h. Therefore, this reaction mixture contains 32.9 mmol of SiO_2, 6.40 mmol of NaOH, and 0.706 mmol of Al_2O_3. Consequently, the molar ratio of SiO_2 to Al_2O_3 in the produced gel is 46.6:1. The produced gel was transferred into 200 mL stainless autoclave maintained at different temperatures: 100, 150 and 180 °C, for 48 h. This hydrothermal reaction was also repeated at 180 °C for 48 h after addition of 5 mL of different organic templates: ethylene glycol, glycerol or polyethylene glycol 200, during the stirring of the reaction blend. After completion of the hydrothermal reaction, the autoclave was naturally cooled. Afterward, the formed precipitates were filtered, washed thoroughly several times with bidistilled water, and dried at 100 °C for 6 h, then calcined at 550 °C for 2 h.

2.3. Adsorption studies

2.3.1. Adsorption of colored compounds from soybean oil

5 mL of crude soybean oil was mixed with 100 mL of n-hexane and kept as a stock solution. Then, for each experiment, 0.2 g of adsorbent (mordenite zeolite which was prepared using PEG 200 (M5 sample) or bleaching earth powder) was added to 20 mL of the stock solution, in Erlenmeyer flasks. Afterword, the suspension was shaken for different time intervals. Aliquots were withdrawn from the flasks, at predefined time intervals, and centrifuged at 2500 rpm. The concentrations of the remaining yellow and red colors in the supernatant were estimated using the UV–Vis spectrophotometer at the corresponding maximum wavelengths; 447 and 474 nm, respectively. The effect of adsorbent dose was also studied using different amounts of the as-prepared zeolite adsorbent or bleaching earth powder (0.05, 0.1, and 0.2 g) at the equilibrium time as previously mentioned. % Removal of yellow and red colors can be calculated using Eq. (1)

$$\%\text{Removal} = [(A_0 - A_t)/A_0]100 \quad (1)$$

where, A_0 is the absorbance of the stock oil solution and A_t is the absorbance of the oil solution after separation of the adsorbent suspension at the desired time.

2.3.2. Adsorption of methylene blue dye from aqueous media

Adsorption properties of the as-fabricated mordenite zeolite toward the removal of MB dye from polluted aqueous media were examined. In the adsorption experiments, 0.1 g of adsorbent (mordenite zeolite prepared using PEG 200 (M5 sample)) was magnetically stirred with 25 mL of MB dye solution (10 mg/L), in Erlenmeyer flasks. The mixture was then stirred at 500 rpm for different times. Aliquots were taken out of the flasks, at pre-defined time intervals, and centrifuged at 2500 rpm. The concentration of the remaining MB dye in the supernatant was estimated using the UV–Vis spectrophotometer at a wavelength of 663 nm. The effect of the adsorbent dose was explored using different quantities of M5 adsorbent (0.025, 0.05, 0.1, 0.125, and 0.18 g) whereas the influence of initial dye concentration was examined employing different concentrations of the dye (10, 25, and 50 mg/L) at the obtained equilibrium time. The effect of temperature (298, 313, and 323 K) on the adsorption process was also examined using 25 mL of MB dye solution (10 mg/L) at the equilibrium time. % Removal of MB dye using M5 adsorbent can be determined using Eq. (2)

$$\%\text{Removal} = [(C_i - C_f)/C_i]100 \quad (2)$$

The adsorption capacity of the M5 adsorbent Q (mg/g) can be estimated employing Eq. (3)

$$Q = (C_i - C_f)V/m \quad (3)$$

where, C_i (mg/L) is the initial concentration of dye solution, C_f (mg/L) is the final concentration of the remaining dye after the adsorption process, V (L) is the volume of dye solution, and m (g) is the mass of M5 adsorbent.

2.4. Physico-chemical measurements

XRD patterns of the as-prepared mordenite samples were determined using an 18 kW diffractometer (Bruker; model D8 Advance) equipped with monochromated Cu K_α radiation (λ) 1.54178 Å. FT-IR spectra of the as-prepared mordenite samples were collected using a Nicolet iSio FT-IR spectrophotometer in the 4000–400 cm^{-1} region using KBr disk. The FE-SEM images of the as-prepared mordenite samples were taken on a scanning electron microscope (JEOL; model JSM5410). Elemental analyses were performed using link, ISIS-300, Oxford EDS (energy dispersion spectroscopy) detector. The HR-TEM images of mordenite sample prepared using polyethylene glycol were collected employing a transmission electron microscope (TEM-2100) at a speeding voltage of 200 kV. The pore size and BET (Brunauer-Emmet-Teller) surface area of the as-fabricated samples were determined by employing nitrogen gas adsorption isotherms on Quantachrome analyzer (Nova 2000 series, USA) at 77 K. The adsorption

investigation was achieved utilizing a UV–visible spectrophotometer (Jasco, model v670).

3. Results and discussion

3.1. XRD study

Fig. 1 exhibits the influence of temperatures: 100, 150, and 180 °C, on the synthesis of mordenite products (M0, M1, and M2, respectively) in the absence of any organic template. The results showed that the hydrothermal treatment at 100 °C produced amorphous products (Fig. 1(A)), and at higher temperatures the reaction gave a crystalline mordenite phase as shown in Fig. 1(B, C). Notably, the mordenite samples produced at 180 °C have a good crystallinity and well-defined phase according to XRD patterns. Therefore, the effect of organic templates: ethylene glycol, glycerol, and polyethylene glycol 200, on the synthesis of mordenite samples has been studied at that temperature (180 °C), and the results are depicted in Fig. 2(A–C), respectively. The relevant mordenite products are labeled as M3, M4, and M5, respectively. The XRD patterns of the obtained products; M1-M5, (Figs. 1 and 2) can be perfectly indexed to the orthorhombic mordenite with cell constants: a = 18.1220 Å, b = 20.2560 Å and c = 7.4730 Å (space group Cmcm, JCPDS card 80–0645). We have not noticed any XRD peaks that can be assigned to other impurities indicating high purity of the as-prepared compounds (M1-M5 samples). The obtained XRD data are in excellent agreement with those have been recently published by Priya et al. [53] and Aly et al. [47]. Employing the Debye–Scherer formula (Eq. (4)), the average crystal sizes of M1-M5 samples were determined using the following equation.

$$D = 0.9\lambda/\beta \cos\theta_B \quad (4)$$

where, λ, θ_B, and β are wavelength of the X-ray radiation, the diffraction angle according to Bragg formula, and the full width at half maximum (FWHM) of the XRD diffraction peaks, respectively. Hence, the calculated average crystallite sizes of mordenite products (M1-M5) were found to be 77.84, 110.5, 73.79, 82.25, and 57.51 nm, respectively. This result shows that the temperature and template type have a significant effect on the crystallite size. When the temperature increased from 150 to 180 °C, the crystallite size of the product enhanced from 77.84 to 110.5 nm,

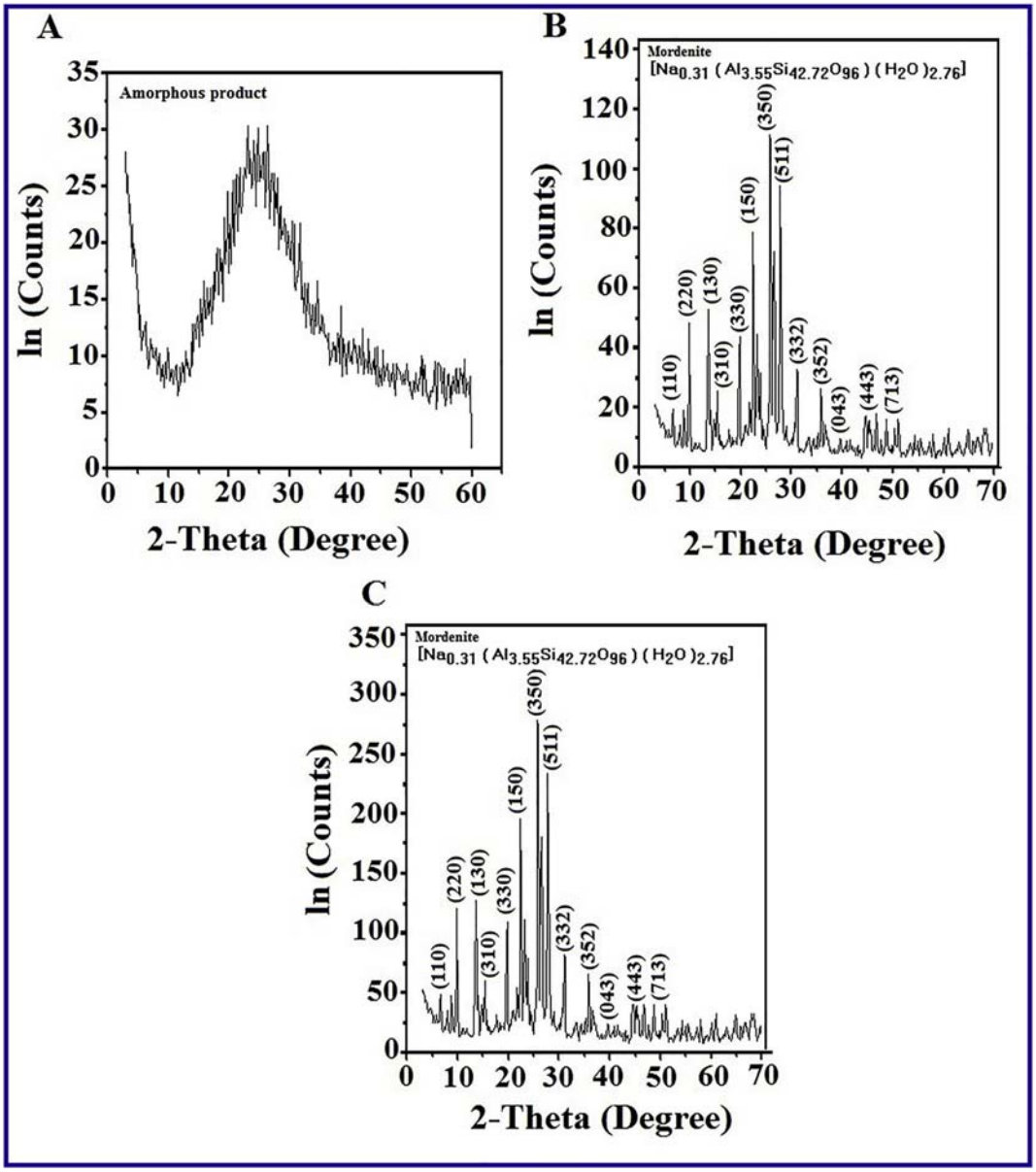

Fig. 1. XRD patterns of the zeolite products prepared in the absence of template at 100 °C (M0 sample) (A), 150 °C (M1 sample) (B), and 180 °C (M2 sample) (C).

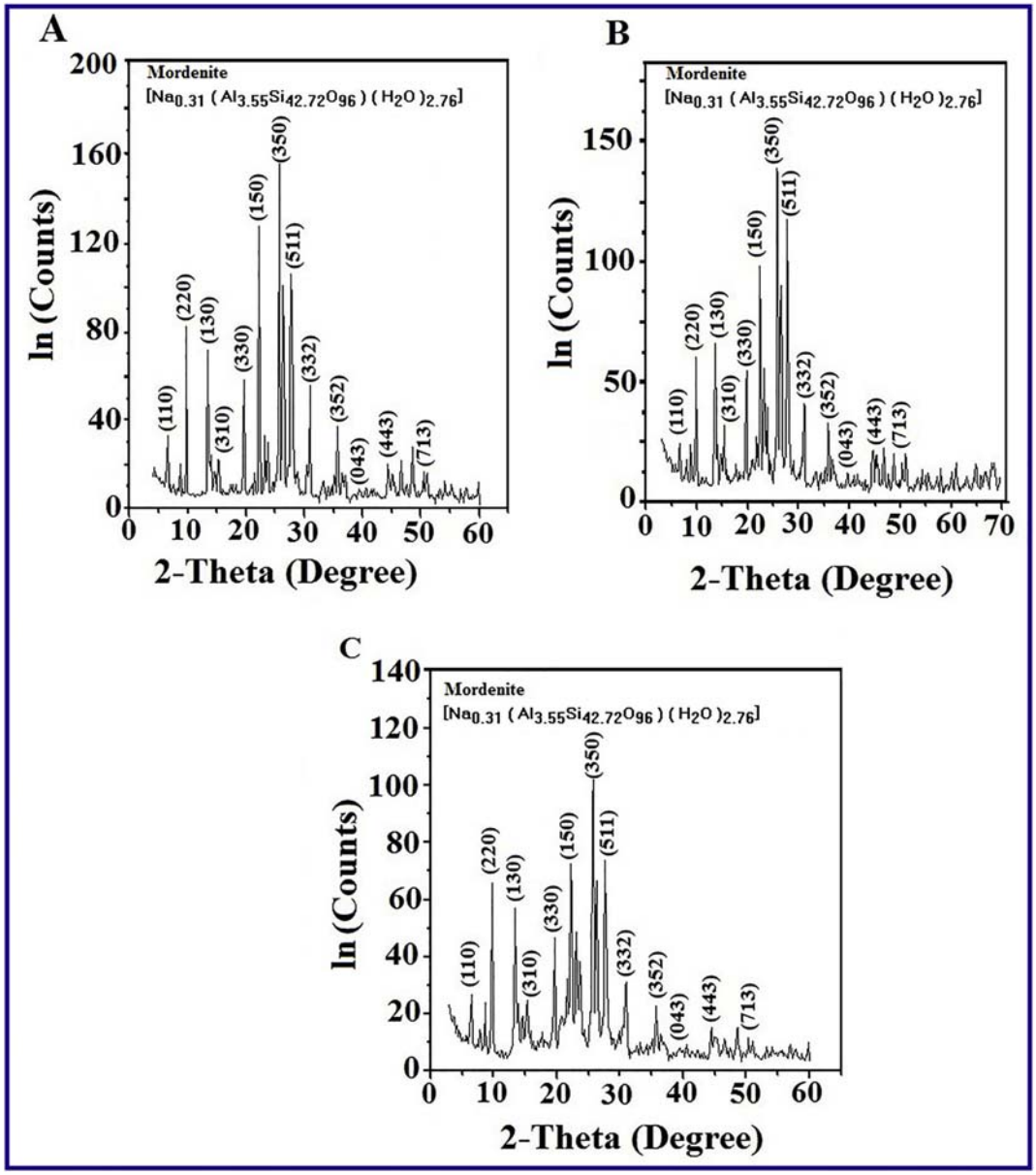

Fig. 2. XRD patterns of the zeolite products prepared using ethylene glycol (M3 sample) (A), glycerol (M4 sample) (B), and PEG 200 (M5 sample) (C).

due to the increase in the rate of crystal growth at higher temperatures. However, addition of organic templates: glycerol, ethylene glycol, and polyethylene glycol 200, to the hydrothermal reaction at 180 °C reduced the crystallite size to 82.25, 73.79, and 57.51 nm, respectively. This is probably due that the organic template direct the reaction and they also may form layers around the formed small particles and preventing them from further growth. These results are in consistent with the published data using other organic templates reported by Priya et al. [53] and Aly et al. [47]. Therefore, we concluded that the optimum conditions for the formation of pure mordenite products with small crystallite sizes were: carrying out the hydrothermal reaction of interest at 180 °C, in the presence of polyethylene glycol 200 as an organic template.

3.2. FT-IR study

The FT-IR spectra of the mordenite products (M2–M5) have been investigated and displayed in Fig. 3(A–D). All the FT-IR spectra of the products showed characteristic vibrations for mordenite: asymmetric stretching: internal at 1021–1025 cm^{-1}, and external at 1215–1226 cm^{-1}; symmetric stretching: internal at 693–709 cm^{-1}, and external at 786–797 cm^{-1}; double ring: at 541–550 and 618–625 cm^{-1}; and T—O bending at 442–459 cm^{-1} [47]. Moreover, the FT-IR spectra of the samples revealed a broad band in the range of 3520–3547 cm^{-1} corresponding to the stretching vibration of the O—H groups of surface adsorbed water molecules. In addition, the spectra also showed absorption bands in the range of 1636–1661 cm^{-1} assigned to H-O-H bending vibrational absorptions [54–59].

3.3. FE-SEM and HR-TEM study

The surface morphologies of the as-fabricated mordenite products: M2–M5, were studied using a field-emission scanning electron microscope (FE-SEM) as shown in Fig. 4(A–D), respectively. The SEM images exhibit that M2 and M5 samples are composed of both of rods agglomerated together in cylindrical shapes with an average size of ca. 622 and 500 nm and spherical shapes of average sizes of ca. 5.2 and 4.3 μm, as displayed in Fig. 4(A) and (D), respectively. The images also revealed that the M3 sample was composed of rods agglomerated together in cylindrical shapes with an average size of ca. 1.6 μm as shown in Fig. 4(B).

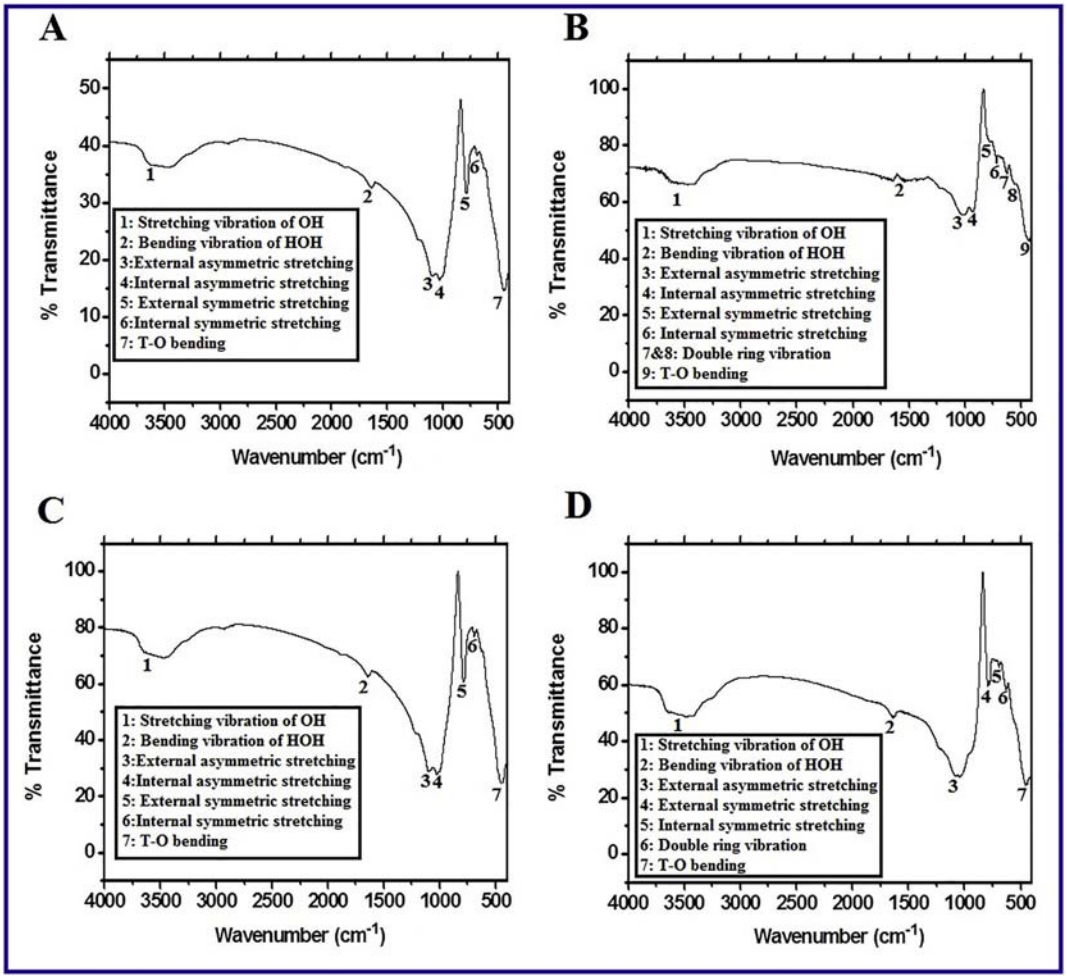

Fig. 3. FT-IR spectra of the zeolite products prepared in the absence of template at 180 °C (M2 sample) (A), as well as in the presence of templates such as ethylene glycol (M3 sample) (B), glycerol (M4 sample) (C), and PEG 200 (M5 sample) (D).

On the other hand, M4 sample was composed of both of rods gathered together in cylindrical, spherical, and cubical shapes with an average size of ca. 550 nm, 5.5 μm, and 1.4 μm, respectively, as presented in Fig. 4(C). Because M5 mordenite sample is the optimized obtained compound, M5 mordenite sample is the only zeolite product in the current study that has been investigated using the TEM and the collected TEM image is displayed in Fig. 4(E). This figure shows that the product consists of irregular, spherical, rods, and network shaped particles with an average diameter of 55.34 nm which coincides with the obtained XRD data. Moreover, energy dispersion spectroscopy (EDS) confirmed the purity of all the prepared mordenite samples through the composition percent's of the Si, Al, Na, and O elements which present in the samples, as shown in Table 1 and Fig. 4(F). The EDS results exhibited that the Si/Al ratio in all of the samples was ca. 8.

3.4. Surface area measurements

Surface area analysis plays a significant role in identifying the characteristics of the prepared compounds by determining the pore size and BET surface area of the as-fabricated products using the N_2 adsorption–desorption isotherm analysis [60]. And the estimated values are presented in Table 2. The results exhibit that the pore size and BET surface area of the as-prepared products increase in the following order M2 < M4 < M1 < M3 < M5. Besides, this can be explained based on that the products crystallite sizes increase in the reverse order.

3.5. Adsorption of yellow and red colors from crude soybean oil using mordenite nanoparticles

The adsorption of yellow and red colors from soybean oil on the as-prepared mordenite nanoparticles (M5), produced from polyethylene glycol 200 template, has been studied because this sample has the lowest crystallite size and the highest surface area. Both the effect of time and M5 adsorbent dose have been studied and compared with bleaching earth powders.

3.5.1. Effect of contact time

The effect of the contact time on the adsorption properties of both bleaching earth powder and M5 adsorbents were studied for the removal of yellow (at 447 nm) and red (at 474 nm) colors, using 0.2 g adsorbents and 20 mL of the stock oil solution, as clarified in Table 3 and Fig. 5. The data revealed that the yellow color removal using M5 and bleaching earth powder adsorbents increased rapidly until it reached ca. 67.98% (Fig. 5B) and 80.08% (Fig. 5A), while those of red color reached ca. 74.15% (Fig. 5B) and 86.00% (Fig. 5A), respectively in 120 min. Then, the percent removal values remained almost constant for 180 min. Hence, the optimum contact time for the colors removal was chosen to be 120 min.

3.5.2. Effect of dose

The influence of the adsorbent dose on the adsorption efficiency of both M5 and bleaching earth powder adsorbents was investigated for

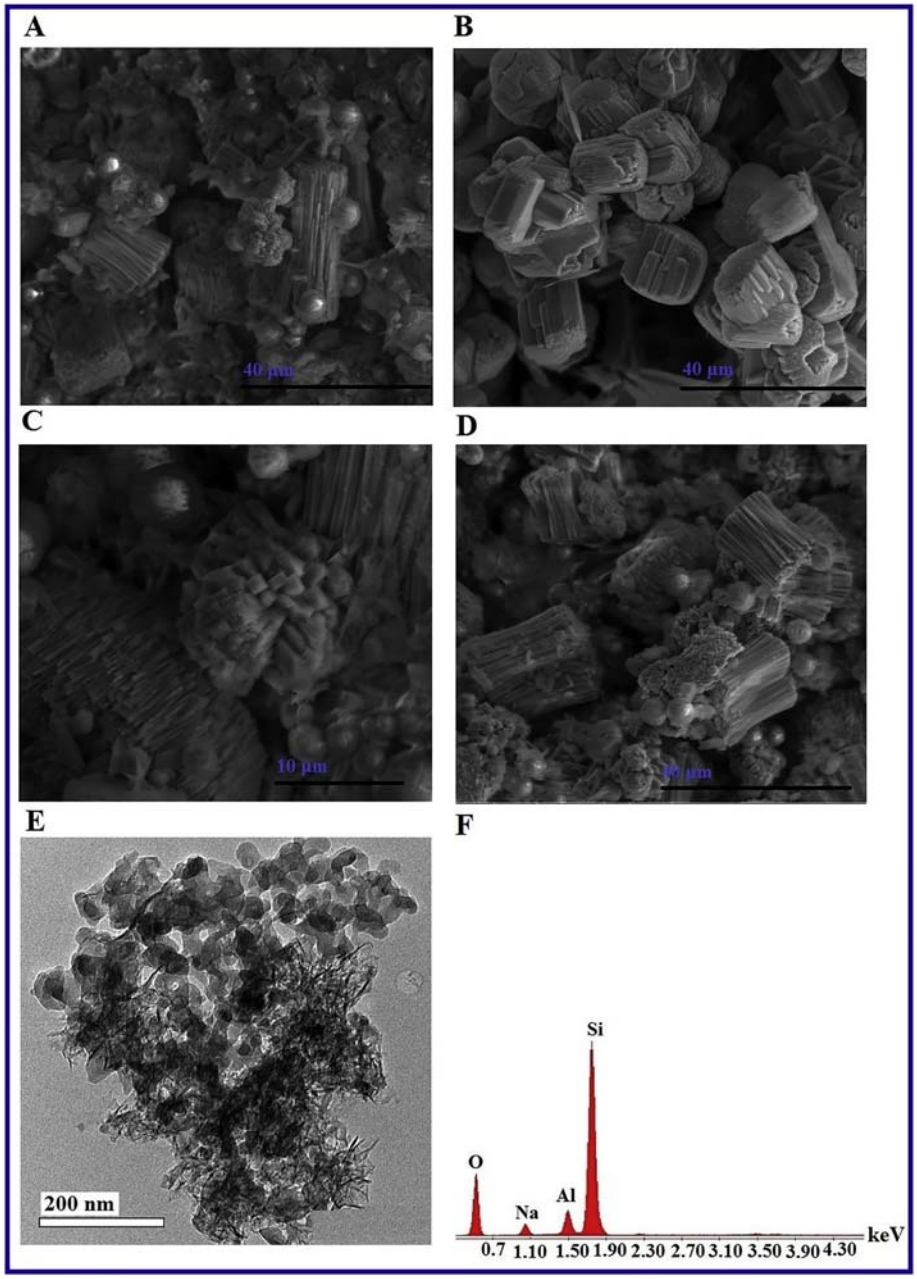

Fig. 4. FE-SEM images of the zeolite products prepared in the absence of template at 180 °C (M2 sample) (A), as well as in the presence of templates such as ethylene glycol (M3 sample) (B), glycerol (M4 sample) (C), and PEG 200 (M5 sample) (D). The TEM image of the zeolite product prepared using PEG 200 (M5 sample) (E), and the EDS spectrum of the zeolite product synthesized using glycerol (M4 sample) (F).

the removal of yellow (at 447 nm) and red (at 474 nm) colors under conditions: 0.05, 0.1, and 0.2 g adsorbents and 20 mL of the stock oil solution for 120 min as presented in Fig. 5 and Table 4. The data revealed that the yellow color removal percentages using 0.05, 0.1, and 0.2 g M5 adsorbent were 20.40%, 27.58%, and 67.98% (Fig. 5D), while those of the bleaching earth powder were 62.12%, 64.40%, and 80.08%, (Fig. 5C), respectively. The data also exhibited that the red color removal percentages using 0.05, 0.1, and 0.2 g M5 adsorbent were 25.92%, 34.69%, and 74.15% (Fig. 5D), while those of bleaching earth powder were 10.64%, 69.11%, and 86.00%, (Fig. 5C), respectively. Thus, the M5 sample shows a comparative adsorption activity to that of the bleaching earth powder. However, the as-prepared M5 sample (mordenite) is

Table 1
EDS data of the prepared samples.

Sample	Si%	Al%	Na%	O%	Si/Al
M2	47.70	5.74	4.32	42.24	8.31
M3	46.85	5.58	4.34	43.23	8.34
M4	46.56	5.47	4.45	43.52	8.51
M5	47.69	5.89	4.26	42.16	8.01

Table 2
BET surface area and pore volume of the prepared samples.

Sample	BET surface area (m^2/g)	Pore volume (cc/g)
M1	20.45	0.0167
M2	15.78	0.0150
M3	24.78	0.0176
M4	20.12	0.0159
M5	28.26	0.0178

Table 3
Effect of contact time on the removal of yellow and red colors from crude soybean oil using bleaching powder and M5 sample.

Time (min)	% Removal of yellow color		% Removal of red color	
	Bleaching powder	Mordenite	Bleaching powder	Mordenite
10	13.42	2.041	12.21	10.64
30	22.70	13.42	24.99	12.21
60	75.92	37.09	80.81	42.98
120	80.08	67.98	86.00	74.15

Where, volume of stock oil solution = 20 mL and mass of the adsorbent = 0.2 g.

Table 4
Effect of the adsorbent dose on the removal of yellow and red colors from crude soybean oil using bleaching powder and M5 sample.

Mass of adsorbent (g)	% Removal of yellow color		% Removal of red color	
	Bleaching powder	Mordenite	Bleaching powder	Mordenite
0.05	62.12	20.40	10.64	25.92
0.1	64.40	27.58	69.11	34.69
0.2	80.08	67.98	86.00	74.15

Where, volume of stock oil solution = 20 mL and contact time = 120 min.

purer and low-cost product on compared to the commercially available bleaching earth powder.

3.6. Adsorption of methylene blue from polluted water using mordentie nanoparticles

The adsorption of MB dye on the as-prepared mordenite nanoparticles (M5) has been studied. The effects of time, temperature, adsorbent dose, and initial dye concentration have been studied.

3.6.1. Effect of contact time and adsorption kinetics

The effect of the contact time on the removal of MB dye using M5 adsorbent was determined at 663 nm utilizing 0.1 g adsorbent and 25 mL of dye solution (10 mg/L) as clarified in Fig. 6. The data revealed that the % removal increased rapidly until it reached ca. 83% (Fig. 6A and C) after 120 min and it remained almost unchanged due to the equilibrium state because of the active sites saturation of the adsorbent. Hence, the optimum contact time was chosen to be 120 min. Studying adsorption kinetics helps with the explanation of adsorption mechanism. In this regard, some kinetic models [23] were applied such as pseudo-first-order (Eq. (5)), pseudo-second-order (Eq. (6)) and intra-particle diffusion (Eq. (7))

$$\log(Q_e - Q_t) = \log Q_e - K_1 t/2.303 \quad (5)$$

$$t/Q_t = \left(1/K_2 Q_e^{\,2}\right) + (1/Q_e)t \quad (6)$$

$$Q_t = K_{int} t^{0.5} + C \quad (7)$$

where, Q_e (mg/g) is the quantity of the adsorbed dye at equilibrium, Q_t (mg/g) is the quantity of the adsorbed dye at time t (min), k_1 (1/min) is the pseudo- first-order rate constant of the adsorption process, k_2 (g/mg·min) is the pseudo-second-order rate constant of the adsorption process, C (mg/g) is the thickness of boundary layer and k_{int} (mg/(g·min$^{0.5}$)) is the internal diffusion constant. The data exhibited that

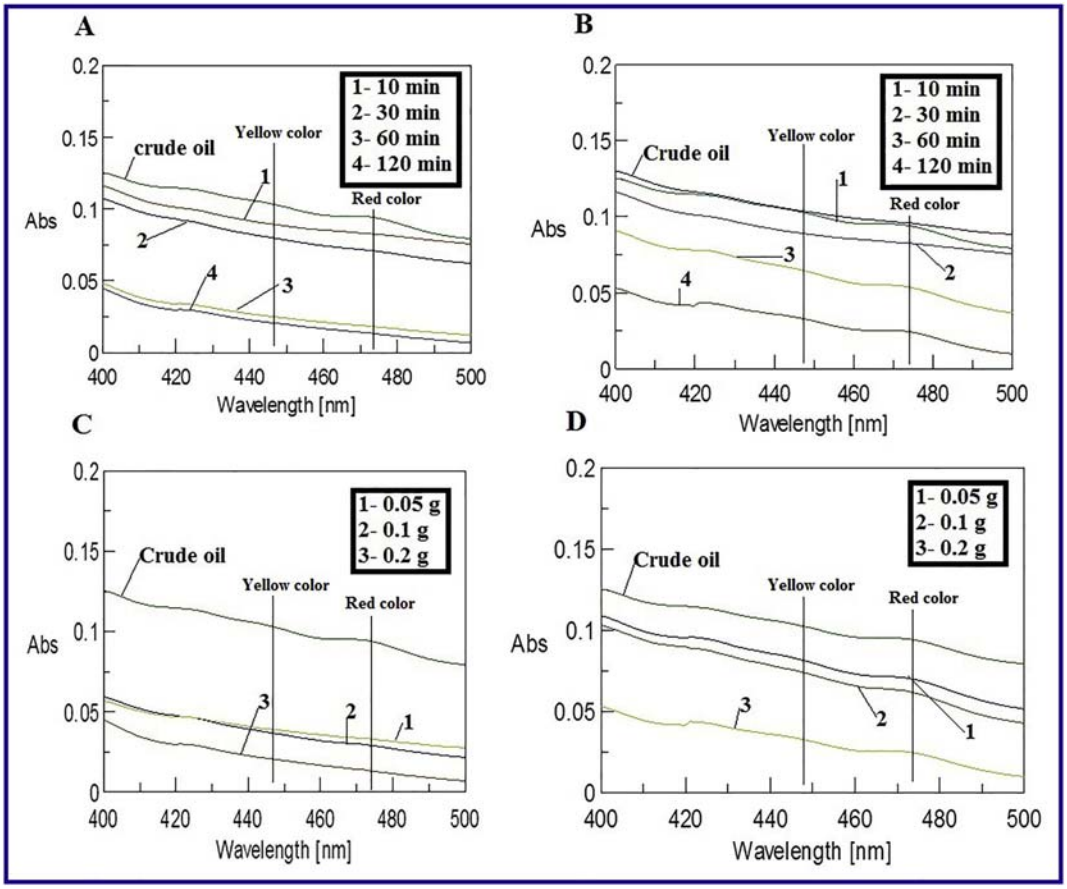

Fig. 5. The effect of contact time on the removal of yellow and red colors from soybean oil using bleaching powder (A) and M5 sample (B), as well as the effect of adsorbent dose on the removal of yellow and red colors from soybean oil using bleaching powder (C) and M5 sample (D). (For interpretation of the references to color in this figure legend, the reader is referred to the web version of this article.)

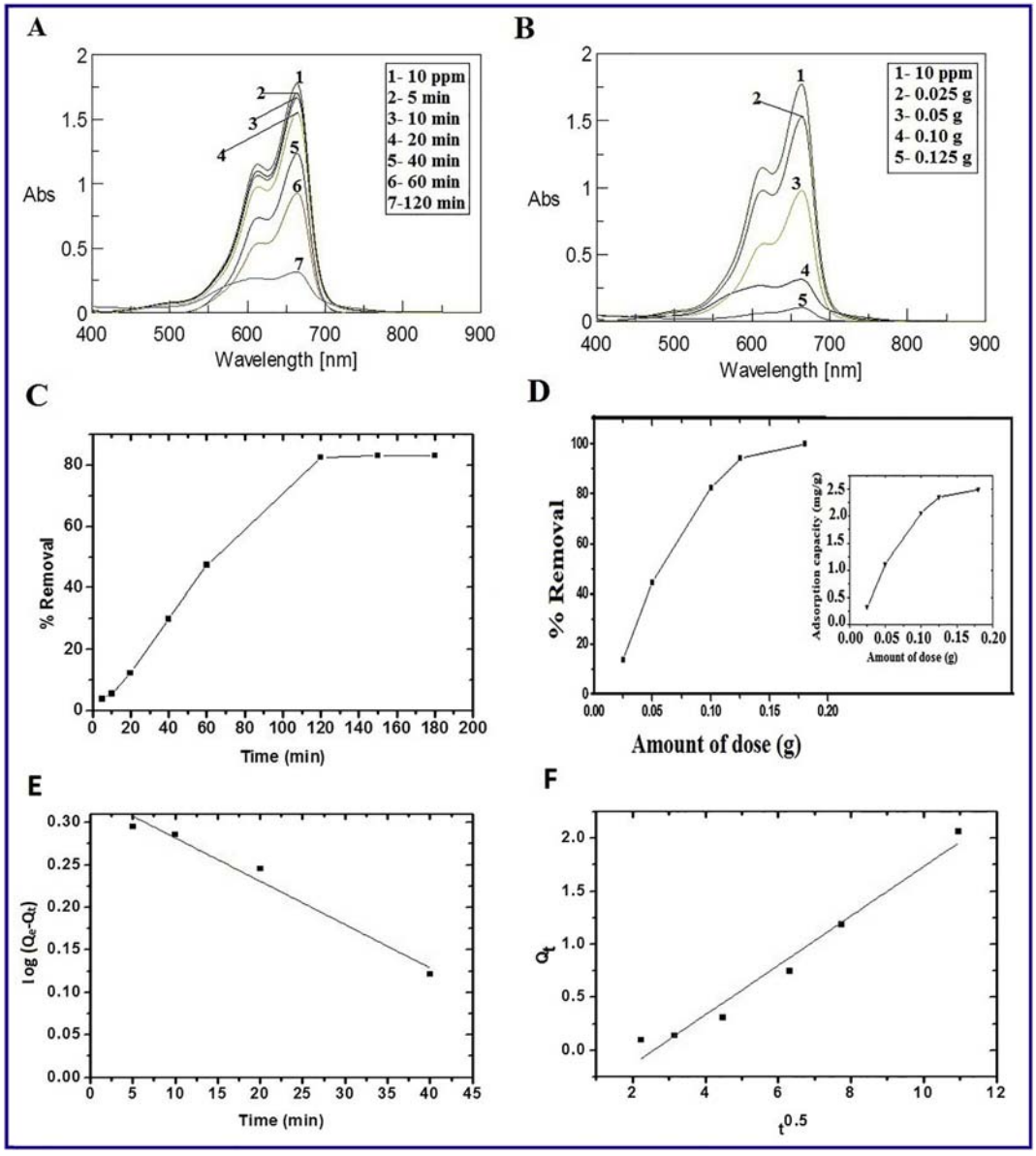

Fig. 6. Effect of contact time on the removal of MB dye using M5 sample (A, C), effect of zeolite dose on the removal of methylene blue dye using M5 sample (B, D), Pseudo first order model (E), and the intra-particle diffusion model (F). (For interpretation of the references to color in this figure legend, the reader is referred to the web version of this article.)

the adsorption process obeys the pseudo-first-order model with a rate constant of 0.012 min^{-1} (Fig. 6E), as it is clear from the value of the correlation coefficients ($R^2 = 0.96$) which is close to unity on comparison to that obtained from the pseudo-second-order ($R^2 = 0.77$) (figure of pseudo-second-order omitted for brevity). Furthermore, the suitability of the pseudo-first-order model was confirmed through the convergence of theoretical and practical results of the calculated adsorption capacity (calc. 2.15 mg/L) (found. 2.07 mg/L). The intra-particle diffusion model assumes that the only rate-controlling process is diffusion within the particles (inner diffusion of adsorbates inside the adsorbent particles). And the zero intercepts of the plot of Q_t vs. $t^{0.5}$ indicates the validity of this model. However, the plot of Q_t vs. $t^{0.5}$ gave linear fitting ($R^2 = 0.96$) which did not pass through the origin (Fig. 6F) with $k_{int} = 0.23$ mg/gmin$^{0.5}$ and $C = 0.59$ mg/g, indicating that intra-particle diffusion is not the only rate-controlling mechanism of MB adsorption onto the M5 but also controlled by some other mechanisms including film diffusion and bulk diffusion [23]. In an attempt to study those other mechanisms, Spahn and Schlunder model (Eq. (8)) was applied to study liquid film diffusion process of adsorbate to the surface of adsorbent from the liquid solution (outer diffusion process) [61].

$$\ln C_t = \ln C_0 - K_{ext} t \tag{8}$$

where, K_{ext} (min^{-1}) is external diffusion constant and C_t (mg/L) is the concentration of dye at time t. It is obvious from Fig. 7A that good linear relationships ($R^2 = 0.97$) between ln C_t and t appeared in the initial 120 min indicating that liquid film diffusion played a dominant part in the primary stage of adsorption process, and the time needed for liquid film diffusion was 120 min. The value of K_{ext} was founded to be 0.0149 min^{-1} whereas C_0 was found 11.50 which was close to the experimental concentration (10 mg/L) indicating the validity of the model. The liquid film diffusion process was also confirmed by the model assumed by Iqbal et al. [62] using Eq. (9) as shown in Fig. 7B.

$$\ln (1 - F) = -K_{ext} t \tag{9}$$

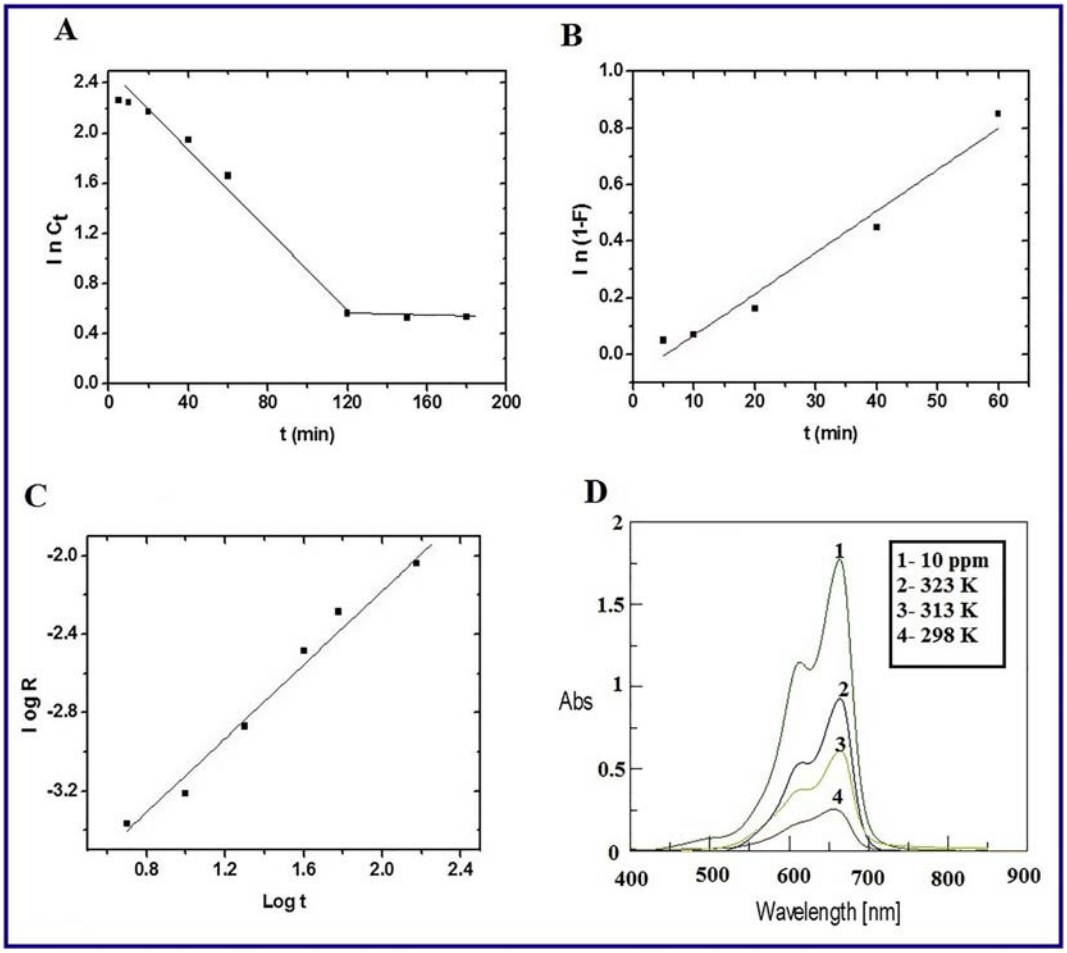

Fig. 7. Spahn and Schlunder model (A), Iqbal model (B), Bingham model (C), and the effect of temperature on the removal of MB dye (D).

where, F is fraction attainment of equilibrium or extent of conversion and it was calculated using Eq. (10)

$$F = Q_t/Q_e \tag{10}$$

It is obvious from Fig. 7B that excellent linear relationships ($R^2 = 0.96$) between ln (1 − F) and t do not pass through the origin indicating that liquid film diffusion played a dominant part in the primary stage of adsorption process. The value of K_{ext} was found to be 0.0147 min^{-1} which was close to that calculated using the Sphan model. In some cases, pore diffusion may be the only rate controlling step. To examine this possibility in the present study, Bangham's equation (Eq. 11) [63] was applied, as presented in Fig. 7C.

$$\log R = \log[K_0\, m/2.303V] + \alpha \log t \tag{11}$$

where, (α (mg/g·min) < 1) and K_0 (g/mg·min) are the Bangham constants. Besides, R can be calculated using Eq. (12)

$$R = \log[C_0/(C_0 - Q_t m)] \tag{12}$$

The plot of log R vs. log t was found to be linear with good correlation coefficient ($R^2 = 0.97$) indicating that the rate determining step is controlled only by the pore diffusion mechanism. Moreover, the values of α and K_0 were 0.9399 mg/g·min and 0.05 g/mg·min, respectively.

Hence, the adsorption of MB dye molecules onto M5 takes place in three successive stages (I) film diffusion: MB adsorbates penetrate to the surface of the zeolite adsorbent across the liquid film, (II) intraparticle diffusion: most MB adsorbates diffuse into the pores inside the adsorbent as the adsorbate molecules are bound or anchored with the active adsorption sites on the zeolite adsorbent surface, and (III) adsorption: adsorption occurs on the inner surface of the zeolite adsorbent. The adsorption rate is usually controlled by the first two stages [63].

3.6.2. Effect of amount of dose

The influence of the amount of dose on the adsorption efficiency of M5 adsorbent was studied using 0.025, 0.05, 0.1, 0.125, and 0.18 g adsorbent and 25 mL of 10 mg/L MB dye solution for 120 min as shown in Fig. 6B and D. The data revealed that the % dye removal was 13.6, 44.6, 82.5, 94.4, and 100%, respectively. Thus, the % dye removal and adsorption capacity increases with increasing the amounts of dose due to increasing the active sites of the used adsorbent.

3.6.3. Effect of concentration and adsorption isotherms

The effect of initial MB dye concentration on the adsorption efficiency of M5 adsorbent was studied at 663 nm by employing 0.1 g of the adsorbent and 25 mL of the dye solutions with initial concentrations of 10, 25, and 50 mg/L, as presented in Fig. 8A. The data showed that the % removal increased as the concentration decreased. Besides, the experimental adsorption data were examined by fitting to Langmuir (Eq. (13)), Freundlich (Eq. (14)), and Dubinin–Radushkevich (Eq. (15)) isotherms [64].

$$C_e/Q_e = (1/bQ_m) + (C_e/Q_m) \tag{13}$$

$$\ln Q_e = \ln K_f + (1/n) \ln C_e \tag{14}$$

$$\ln Q_e = \ln Q_m - K_{DR}\varepsilon^2 \tag{15}$$

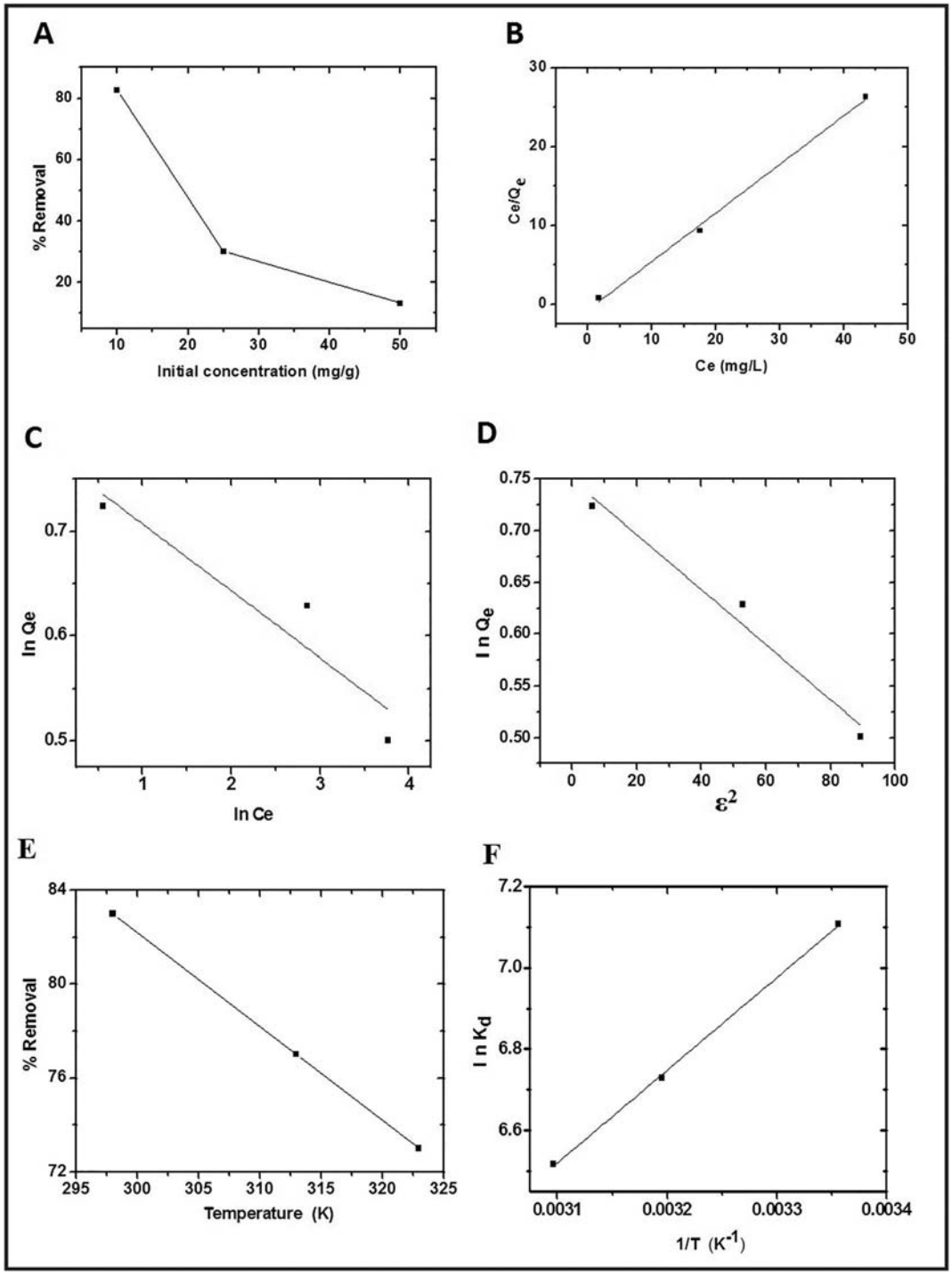

Fig. 8. Effect of the initial concentrations on the removal of MB dye (A), Langmuir isotherm (B), Freundlish isotherm (C), Dubinin–Radushkevich isotherm (D), plot of % removal of methylene blue dye vs. temperature (E), and plot of $\ln K_d$ vs. 1/T (F). (For interpretation of the references to color in this figure legend, the reader is referred to the web version of this article.)

where, Q_e (mg/g) is the quantity of the adsorbed dye at the equilibrium, C_e (mg/L) is the remained dye concentration in the solutions at the equilibrium, Q_m (mg/g) is the maximum sorption capacity, b (L/mg) is the Langmuir constant, K_f (mg/g)(L/mg)$^{1/n}$ is the Freundlish constant, 1 / n is the heterogeneity factor, K_{DR} (mol^2/KJ^2) is DR constant and ε is the Polanyi potential (logarithmic function of adsorbate concentration) which is given by Eq. (16)

$$\varepsilon = RT\,Ln\,[1/(1+C_e)] \quad (16)$$

The Langmuir isotherm model suggests that the adsorption sites on zeolite adsorbent are equivalent (homogenous zeolite surface) and the binding ability of an ion is independent of whether the neighboring sites are occupied or not (i.e. monolayer model predicting saturation of the zeolite adsorbent by MB adsorbate molecules). Once a site is occupied, then no further adsorption on that site can occur [23]. The data were drawn as shown in Fig. 8B. Based on this, the values of Q_m, b, and correlation co-efficient (R^2) were 1.72 mg/g, 0.89 (L/mg), and 0.99, respectively. Freundlich isotherm refers to physical adsorption on heterogeneous zeolite surfaces and it is applicable to multilayer

Table 5
Thermodynamic parameters of the adsorption of MB dye on the as-prepared zeolite product.

Temperature (k)	ΔG^o (KJ/mol)	ΔS^o (KJ/mol K)	ΔH^o (KJ/mol)
298	−17.60	−0.0046	−18.98
313	1.443	–	–
323	1.489	–	–

adsorptions [23]. The data drawn, as shown in Fig. 8C, show that the values of Q_m, 1 / n, K_f, and correlation co-efficient (R^2) were 2.5 mg/g, 0.06, 2.2 (mg/g)(L/mg)$^{1/n}$, and 0.79, respectively. It is noteworthy that Q_m can be calculated from Freundlish isotherm, using Eq. (17), as reported by Halsey [23].

$$Q_m = K_f(C_o)^{1/n} \quad (17)$$

Based on the aforementioned discussion, we concluded that the adsorption experimental results fitted well the Langmuir isotherm model because the corresponding correlation co-efficient is closer to unity compared to that obtained from the Freundlish isotherm model. Moreover, Q_m value calculated from the Langmuir isotherm model (1.72 mg/g) is close to the experimentally calculated value (1.86 mg/g) which is considered to be a relatively high compared to those of other zeolites reported in the literatures [65]. Dubinin–Radushkevich (D–R) isotherm was used to understand the type of bonding between MB dye and M5 i.e. chemical or physical [64]. The data estimated from Fig. 8D show that the values of Q_m, K_{DR}, and correlation co-efficient (R^2) were 2.12 mg/g, 0.0026 mol^2/KJ^2, and 0.95, respectively. It is noteworthy that mean energy of sorption (E) was calculated using Eq. (18)

$$E = 1/(2K_{DR})^{0.5} \quad (18)$$

It was found that E = 13.8 KJ/mol indicating that the type of adsorption is a physical adsorption process [24,64].

3.6.4. Effect of temperature and adsorption thermodynamic parameters

The influence of temperature on the adsorption process was explored. The experimental results exhibited that the adsorption efficiency decreased largely with raising the temperature of the adsorption media, as depicted in Figs. 7D and 8E. The % dye removal at 298, 313, and 323 K were ca. 83, 77, and 73%, respectively. Hence, the results revealed that the adsorption process was an exothermic process. The reduction in the adsorption rate with raising the temperature may be due to that the MB dye molecules at higher temperatures have a great ability to being de-adsorbed and escaped to the liquid phase [23]. Thermodynamic constants such as a change in free energy (ΔG^o), change in enthalpy (ΔH^o), and change in the entropy (ΔS^o) were determined using Eqs. (19) and (20) [23].

$$\ln K_d = (\Delta S^o/R) - (\Delta H^o/RT) \quad (19)$$

$$\Delta G^o = \Delta H^o - T\Delta S^o \quad (20)$$

where, T (K) is temperature, R (KJ/mol K) is gas constant and K_d (L/g) is distribution co-efficient which is calculated from Eqs. (21) or (22)

$$K_d = Q_e/C_e \quad (21)$$
$$K_d = [\%\text{removal}/(100 - \%\text{removal})]V/m \quad (22)$$

It is clearly seen from Fig. 8F and Table 5 that the adsorption of MB dye on the prepared mordenite adsorbent is spontaneous (feasible) at lower temperatures and exothermic process due to the obtained negative ΔG^o and ΔH^o values of this process, respectively. Besides, the process is non-spontaneous (not feasible) at higher temperatures due to the positive values of ΔG^o. Moreover, the adsorption of MB dye on the prepared mordenite adsorbent is physisorption because the ΔH^o value is −18.98 kJ/mol [23,24], which is considered in excellent accordance with the previously calculated data using the DR isotherm model. Eventually, mordenite zeolite was expected to be a promising adsorbent and have the potential to be used as low-cost adsorbents for wastewater treatment.

4. Conclusion

In summary, mordenite zeolite nanoparticles were synthesized via a low-cost hydrothermal method in the absence and presence of organic templates (ethylene glycol, glycerol and polyethylene glycol 200). The average crystallite size of the prepared mordenite samples was increased in the following order: M5 (PEG 200) < M3 (ethylene glycol) < M4 (glycerol) < M2 (without template). The type of organic templates has a great effect on the phase purity, crystallite size, and morphology of the prepared nano-sized mordenite samples. Polyethylene glycol 200 organic template produced mordenite product with the smallest crystallite size particles. The as-prepared mordenite product showed good adsorption efficiency for the removal of yellow and red colors from soybean crude oil, and it gave good results in comparison to the commercially available bleaching earth powder. The as-prepared mordenite product also revealed good efficiency toward the removal of methylene blue (MB) dye from polluted aqueous solutions. The adsorption process followed pseudo-first-order, intra-particle diffusion, liquid film diffusion and pore diffusion model whereas rate determining step is controlled by the pore diffusion model. The adsorption data fitted well both Langmuir and Dubinin–Radushkevich (D–R) isotherms. In addition, the adsorption of MB dye on the as-prepared mordenite adsorbent is spontaneous and exothermic at lower temperatures attributing to the obtained negative ΔG^o and ΔH^o values, respectively. Besides, the process is non-spontaneous (not feasible) at higher temperatures due to the positive values of ΔG^o. Moreover, the adsorption of MB dye on the prepared mordenite adsorbent is a physisorption process.

Acknowledgements

The authors are grateful to Benha University, Egypt.

References

[1] S. Bhardwaj, S.J. Passi, A. Misra, K.K. Pant, K. Anwar, R.M. Pandey, V. Kardam, Effect of heating/reheating of fats/oils, as used by Asian Indians, on trans fatty acid formation, Food Chem. 212 (2016) 663–670.
[2] R. Nur Fatin Nazurah, Z.A. Nur Hanani, Physicochemical characterization of kappa-carrageenan (*Euchema cottoni*) based films incorporated with various plant oils, Carbohydr. Polym. 157 (2017) 1479–1487.
[3] G. Tian, W. Wang, B. Mu, Y. Kang, A. Wang, Facile fabrication of carbon/attapulgite composite for bleaching of palm oil, J. Taiwan Inst. Chem. Eng. 50 (2015) 252–258.
[4] E.A. Vlasova, S.A. Yakimov, E.V. Naidenko, E.V. Kudrik, S.V. Makarov, Application of metal-organic frameworks for purification of vegetable oils, Food Chem. 190 (2016) 103–109.
[5] Y. Bayrak, Adsorption isotherms in bleaching hazelnut oil, J. Am. Oil Chem. Soc. 80 (2003) 1143–1146.
[6] Y. Liu, J. Huang, X. Wang, Adsorption isotherms for bleaching soybean oil with activated attapulgite, J. Am. Oil Chem. Soc. 85 (2008) 979–984.
[7] D. Su, T. Xiao, D. Gu, Y. Cao, Y. Jin, W. Zhang, T. Wu, Ultrasonic bleaching of rapeseed oil: effects of bleaching conditions and underlying mechanisms, J. Food Eng. 117 (2013) 8–13.
[8] S.M. Silva, K.A. Sampaio, R. Ceriani, R. Verhé, C. Stevens, W. De Greyt, A.J.A. Meirelles, Adsorption of carotenes and phosphorus from palm oil onto acid activated bleaching earth: equilibrium, kinetics and thermodynamics, J. Food Eng. 118 (2013) 341–349.
[9] P.J. García-Moreno, A. Guadix, L. Gómez-Robledo, M. Melgosa, E.M. Guadix, Optimization of bleaching conditions for sardine oil, J. Food Eng. 116 (2013) 606–612.
[10] M.O. Caglayan, S. Kafa, N. Yigit, Al-pillared clay for cottonseed oil bleaching: an optimization study, J. Am. Oil Chem. Soc. 82 (2005) 599–602.
[11] N. Worasith, B.A. Goodman, N. Jeyashoke, P. Thiravetyan, Decolorization of rice bran oil using modified kaolin, J. Am. Oil Chem. Soc. 88 (2011) 2005–2014.
[12] M.Y. Nassar, M.M. Moustafa, M.M. Taha, Hydrothermal tuning of the morphology and particle size of hydrozincite nanoparticles using different counterions to

produce nanosized ZnO as an efficient adsorbent for textile dye removal, RSC Adv. 6 (2016) 42180–42195.
[13] N.F. Cardoso, R.B. Pinto, E.C. Lima, T. Calvete, C.V. Amavisca, B. Royer, M.L. Cunha, T.H.M. Fernandes, I.S. Pinto, Removal of remazol black B textile dye from aqueous solution by adsorption, Desalination 269 (2011) 92–103.
[14] B. Kayan, B. Gözmen, M. Demirel, A.M. Gizir, Degradation of acid red 97 dye in aqueous medium using wet oxidation and electro-Fenton techniques, J. Hazard. Mater. 177 (2010) 95–102.
[15] M.Y. Nassar, T.Y. Mohamed, I.S. Ahmed, N.M. Mohamed, M. Khatab, Hydrothermally synthesized Co_3O_4, α-Fe_2O_3, and $CoFe_2O_4$ nanostructures: efficient nano-adsorbents for the removal of Orange G textile dye from aqueous media, J Inorg Organomet Polym 27 (2017) 1526–1537.
[16] M.Y. Nassar, I.S. Ahmed, I. Samir, A novel synthetic route for magnesium aluminate ($MgAl_2O_4$) nanoparticles using sol–gel auto combustion method and their photocatalytic properties, Spectrochim. Acta A Mol. Biomol. Spectrosc. 131 (2014) 329–334.
[17] M. Djenouhat, O. Hamdaoui, M. Chiha, M.H. Samar, Ultrasonication-assisted preparation of water-in-oil emulsions and application to the removal of cationic dyes from water by emulsion liquid membrane: part 2. Permeation and stripping, Sep. Purif. Technol. 63 (2008) 231–238.
[18] A.B. Fradj, S.B. Hamouda, H. Ouni, R. Lafi, L. Gzara, A. Hafiane, Removal of methylene blue from aqueous solutions by poly(acrylic acid) and poly(ammonium acrylate) assisted ultrafiltration, Sep. Purif. Technol. 133 (2014) 76–81.
[19] D. Robati, M. Rajabi, O. Moradi, F. Najafi, I. Tyagi, S. Agarwal, V.K. Gupta, Kinetics and thermodynamics of malachite green dye adsorption from aqueous solutions on graphene oxide and reduced graphene oxide, J. Mol. Liq. 214 (2016) 259–263.
[20] E. Pajootan, M. Arami, N.M. Mahmoodi, Binary system dye removal by electrocoagulation from synthetic and real colored wastewaters, J. Taiwan Inst. Chem. Eng. 43 (2012) 282–290.
[21] Q. Wu, W.-T. Li, W.-H. Yu, Y. Li, A.-M. Li, Removal of fluorescent dissolved organic matter in biologically treated textile wastewater by ozonation-biological aerated filter, J. Taiwan Inst. Chem. Eng. 59 (2016) 359–364.
[22] A. Mohammadzadeh, M. Ramezani, A.M. Ghaedi, Synthesis and characterization of Fe_2O_3–ZnO–$ZnFe_2O_4$/carbon nanocomposite and its application to removal of bromophenol blue dye using ultrasonic assisted method: optimization by response surface methodology and genetic algorithm, J. Taiwan Inst. Chem. Eng. 59 (2016) 275–284.
[23] M.Y. Nassar, T.Y. Mohamed, I.S. Ahmed, I. Samir, MgO nanostructure via a sol-gel combustion synthesis method using different fuels: an efficient nano-adsorbent for the removal of some anionic textile dyes, J. Mol. Liq. 225 (2017) 730–740.
[24] M.Y. Nassar, E.I. Ali, E.S. Zakaria, Tunable auto-combustion preparation of TiO_2 nanostructures as efficient adsorbents for the removal of an anionic textile dye, RSC Adv. 7 (2017) 8034–8050.
[25] M.Y. Nassar, M. Khatab, Cobalt ferrite nanoparticles via a template-free hydrothermal route as an efficient nano-adsorbent for potential textile dye removal, RSC Adv. 6 (2016) 79688–79705.
[26] M.Y. Nassar, A.A. Ali, A.S. Amin, A facile Pechini sol–gel synthesis of TiO_2/Zn_2TiO_2/ZnO/C nanocomposite: an efficient catalyst for the photocatalytic degradation of Orange G textile dye, RSC Adv. 7 (2017) 30411–30421.
[27] M.Y. Nassar, S. Abdallah, Facile controllable hydrothermal route for a porous $CoMn_2O_4$ nanostructure: synthesis, characterization, and textile dye removal from aqueous media, RSC Adv. 6 (2016) 84050–84067.
[28] H.M. Aly, M.E. Moustafa, M.Y. Nassar, E.A. Abdelrahman, Synthesis and characterization of novel Cu (II) complexes with 3-substituted-4-amino-5-mercapto-1,2,4-triazole Schiff bases: a new route to CuO nanoparticles, J. Mol. Struct. 1086 (2015) 223–231.
[29] M.Y. Nassar, I.S. Ahmed, Template-free hydrothermal derived cobalt oxide nanopowders: synthesis, characterization, and removal of organic dyes, Mater. Res. Bull. 47 (2012) 2638–2645.
[30] M.Y. Nassar, I.S. Ahmed, Hydrothermal synthesis of cobalt carbonates using different counter ions: an efficient precursor to nano-sized cobalt oxide (Co_3O_4), Polyhedron 30 (2011) 2431–2437.
[31] W. Wang, T. Jiao, Q. Zhang, X. Luo, J. Hu, Y. Chen, Q. Peng, X. Yan, B. Li, Hydrothermal synthesis of hierarchical core-shell manganese oxide nanocomposites as efficient dye adsorbents for wastewater treatment, RSC Adv. 5 (2015) 56279–56285.
[32] H. Guo, T. Jiao, Q. Zhang, W. Guo, Q. Peng, X. Yan, Preparation of graphene oxide-based hydrogels as efficient dye adsorbents for wastewater treatment, Nanoscale Res. Lett. 10 (2015) 1–10.
[33] K. Leng, Y. Sun, X. Zhang, M. Yu, W. Xu, Ti-modified hierarchical mordenite as highly active catalyst for oxidative desulfurization of dibenzothiophene, Fuel 174 (2016) 9–16.
[34] A.N.C. van Laak, S.L. Sagala, J. Zečević, H. Friedrich, P.E. de Jongh, K.P. de Jong, Mesoporous mordenites obtained by sequential acid and alkaline treatments – catalysts for cumene production with enhanced accessibility, J. Catal. 276 (2010) 170–180.
[35] A. Martucci, L. Pasti, M. Nassi, A. Alberti, R. Arletti, R. Bagatin, R. Vignola, R. Sticca, Adsorption mechanism of 1,2-dichloroethane into an organophilic zeolite mordenite: a combined diffractometric and gas chromatographic study, Microporous Mesoporous Mater. 151 (2012) 358–367.
[36] P. Simoncic, T. Armbruster, Cationic methylene blue incorporated into zeolite mordenite-Na: a single crystal X-ray study, Microporous Mesoporous Mater. 81 (2005) 87–95.
[37] A. Gładysz-Płaska, M. Majdan, S. Pikus, Adsorption of lanthanides on mordenite from nitrate medium, J. Colloid Interface Sci. 317 (2008) 409–423.
[38] L. Pasti, E. Rodeghero, E. Sarti, V. Bosi, A. Cavazzini, R. Bagatin, A. Martucci, Competitive adsorption of VOCs from binary aqueous mixtures on zeolite ZSM-5, RSC Adv. 6 (2016) 54544–54552.
[39] M.J.F. Costa, J. Marszewska, A.A.S. Goncalves, L.K.C. de Souza, A.S. Araujo, M. Jaroniec, Microwave-assisted single-surfactant templating synthesis of mesoporous zeolites, RSC Adv. 6 (2016) 54956–54963.
[40] J.P. Soetardji, J.C. Claudia, Y.-H. Ju, J.A. Hriljac, T.-Y. Chen, F.E. Soetaredjo, S.P. Santoso, A. Kurniawan, S. Ismadji, Ammonia removal from water using sodium hydroxide modified zeolite mordenite, RSC Adv. 5 (2015) 83689–83699.
[41] S. Sen Gupta, K.G. Bhattacharyya, Adsorption of metal ions by clays and inorganic solids, RSC Adv. 4 (2014) 28537–28586.
[42] M.Y. Nassar, E.A. Abdelrahman, Hydrothermal tuning of the morphology and crystallite size of zeolite nanostructures for simultaneous adsorption and photocatalytic degradation of methylene blue dye, J. Mol. Liq. 242 (2017) 364–374.
[43] X. Li, R. Prins, J.A. van Bokhoven, Synthesis and characterization of mesoporous mordenite, J. Catal. 262 (2009) 257–265.
[44] K.Y. Lee, M. Park, J. Kim, M. Oh, E.H. Lee, K.W. Kim, D.Y. Chung, J.K. Moon, Equilibrium, kinetic and thermodynamic study of cesium adsorption onto nanocrystalline mordenite from high-salt solution, Chemosphere 150 (2016) 765–771.
[45] S. Samanta, N.K. Mal, P. Kumar, A. Bhaumik, Hydrothermally synthesized high silica mordenite as an efficient catalyst in alkylation reaction under liquid phase condition, J. Mol. Catal. A Chem. 215 (2004) 169–175.
[46] M.M. Mohamed, T.M. Salama, I. Othman, I.A. Ellah, Synthesis of high silica mordenite nanocrystals using o-phenylenediamine template, Microporous Mesoporous Mater. 84 (2005) 84–96.
[47] H.M. Aly, M.E. Moustafa, E.A. Abdelrahman, Synthesis of mordenite zeolite in absence of organic template, Adv. Powder Technol. 23 (2012) 757–760.
[48] L. Zhang, A.N.C.v. Laak, P.E.d. Jongh, K.P.d. Jong, Synthesis of large mordenite crystals with different aspect ratios, Microporous Mesoporous Mater. 126 (2009) 115–124.
[49] Y. Yuan, L. Wang, H. Liu, P. Tian, M. Yang, S. Xu, Z. Liu, Facile preparation of nanocrystal-assembled hierarchical mordenite zeolites with remarkable catalytic performance, Chin. J. Catal. 36 (2015) 1910–1919.
[50] A. Lv, H. Xu, H. Wu, Y. Liu, P. Wu, Hydrothermal synthesis of high-silica mordenite by dual-templating method, Microporous Mesoporous Mater. 145 (2011) 80–86.
[51] M.Y. Nassar, Size-controlled synthesis of $CoCO_3$ and Co_3O_4 nanoparticles by free-surfactant hydrothermal method, Mater. Lett. 94 (2013) 112–115.
[52] M.Y. Nassar, T.Y. Mohamed, I.S. Ahmed, One-pot solvothermal synthesis of novel cobalt salicylaldimine–urea complexes: a new approach to Co_3O_4 nanoparticles, J. Mol. Struct. 1050 (2013) 81–87.
[53] S.S. Priya, P. Bhanuchander, V.P. Kumar, D.K. Dumbre, S.R. Periasamy, S.K. Bhargava, M. Lakshmi Kantam, K.V.R. Chary, Platinum supported on H-mordenite: a highly efficient catalyst for selective hydrogenolysis of glycerol to 1,3-propanediol, ACS Sustain. Chem. Eng. 4 (2016) 1212–1222.
[54] M.Y. Nassar, I.S. Ahmed, T.Y. Mohamed, M. Khatab, A controlled, template-free, and hydrothermal synthesis route to sphere-like α-Fe_2O_3 nanostructures for textile dye removal, RSC Adv. 6 (2016) 20001–20013.
[55] M.Y. Nassar, I.S. Ahmed, I. Samir, A novel synthetic route for magnesium aluminate ($MgAl_2O_4$) nanoparticles using sol-gel auto combustion method and their photocatalytic properties, Spectrochim. Acta A Mol. Biomol. Spectrosc. 131 (2014) 329–334.
[56] M.Y. Nassar, H.M. Aly, E.A. Abdelrahman, Moustafa M.E., Synthesis, characterization, and biological activity of some novel Schiff bases and their Co(II) and Ni(II) complexes: a new route for Co_3O_4 and NiO nanoparticles for photocatalytic degradation of methylene blue dye, J. Mol. Struct. 1143 (2017) 462–471.
[57] M.Y. Nassar, E.A. El-Moety, M.F. El-Shahat, Synthesis and characterization of a $ZnMn_2O_4$ nanostructure as a chemical nanosensor: a facile and new approach for colorimetric determination of omeprazole and lansoprazole drugs, RSC Adv. 7 (2017) 43798–43811.
[58] M. Mostafa, H.M. Saber, A.A. El-Sadek, M.Y. Nassar, Preparation and performance of 99Mo/99mTc chromatographic column generator based on zirconium molybdosilicate, Radiochimica Acta 2016, pp. 257–265.
[59] M.Y. Nassar, A.S. Attia, K.A. Alfallous, M.F. El-Shahat, Synthesis of two novel dinuclear molybdenum(0) complexes of quinoxaline-2,3-dione: new precursors for preparation of α-MoO_3 nanoplates, Inorg. Chim. Acta 405 (2013) 362–367.
[60] Y. Ji, B. Shi, H. Yang, W. Yan, Synthesis of isomorphous MFI nanosheet zeolites for supercritical catalytic cracking of n-dodecane, Appl. Catal. A Gen. 533 (2017) 90–98.
[61] Y. Wu, M. Zhang, H. Zhao, S. Yang, A. Arkin, Functionalized mesoporous silica material and anionic dye adsorption: MCM-41 incorporated with amine groups for competitive adsorption of Acid Fuchsine and Acid Orange II, RSC Adv. 4 (2014) 61256–61267.
[62] D.M.R.E.A. Dissanayake, W.M.K.E.H. Wijesinghe, S.S. Iqbal, N. Priyantha, M.C.M. Iqbal, Fuchsine biosorption using Asplenium nidus biosorbent-a mechanism using kinetic and isotherm data, RSC Adv. 6 (2016) 98682–98692.
[63] V. Srivastava, P. Maydannik, Y.C. Sharma, M. Sillanpää, Synthesis and application of polypyrrole coated tenorite nanoparticles (PPy@TN) for the removal of the anionic food dye 'tartrazine' and divalent metallic ions viz. Pb(ii), Cd(ii), Zn(ii), Co(ii), Mn(ii) from synthetic wastewater, RSC Adv. 5 (2015) 80829–80843.
[64] S.A. Chaudhry, M. Ahmed, S.I. Siddiqui, S. Ahmed, Fe(III)–Sn(IV) mixed binary oxide-coated sand preparation and its use for the removal of As(III) and As(V) from water: application of isotherm, kinetic and thermodynamics, J. Mol. Liq. 224 (2016) 431–441.
[65] K.Y. Hor, J.M.C. Chee, M.N. Chong, B. Jin, C. Saint, P.E. Poh, R. Aryal, Evaluation of physicochemical methods in enhancing the adsorption performance of natural zeolite as low-cost adsorbent of methylene blue dye from wastewater, J. Clean. Prod. 118 (2016) 197–209.